# Electron Donor−Acceptor Interactions in Ethanol−$CO_2$ Mixtures: An Ab Initio Molecular Dynamics Study of Supercritical Carbon Dioxide†

**Moumita Saharay‡ and Sundaram Balasubramanian***

*Chemistry and Physics of Materials Unit, Jawaharlal Nehru Centre for Advanced Scientific Research, Jakkur, Bangalore 560 064, India*

*Received: July 13, 2005; In Final Form: September 30, 2005*

The nature of interactions between ethanol and carbon dioxide has been characterized using simulations via the Car−Parrinello molecular dynamics (CPMD) method. Optimized geometries and energetics of free-standing ethanol−$CO_2$ clusters exhibit evidence for a relatively more stable electron donor−acceptor (EDA) complex between these two species rather than a hydrogen-bonded configuration. This fact has also been confirmed by the higher formation rate of the EDA complex in supercritical carbon dioxide−ethanol mixtures. The probability density distribution of $CO_2$ molecules around ethanol in the supercritical state shows two high probability regions along the direction of the lone pairs on the oxygen atom of ethanol. The EDA interaction between ethanol and $CO_2$ as well as that between $CO_2$ molecules themselves leads to significant deviations from linearity in the geometry of the $CO_2$ molecule. The vibrational spectra of carbon dioxide obtained from the atomic velocity correlation functions in the bulk system as well as from isolated complexes show splitting of the $\nu_2$ bending mode that arises largely from $CO_2$−$CO_2$ interactions, with ethanol contributing only marginally because of its low concentration in the present study. The stretching frequency of the hydroxyl group of ethanol is shifted to lower frequencies in the bulk mixture when compared to its gas-phase value, in agreement with experiments.

## 1. Introduction

Supercritical carbon dioxide ($scCO_2$) is an environmentally benign "green solvent"[1−4] because of its nontoxicity, recyclability, high diffusivity, and tunability of solvent properties. A serious limitation in the application of $scCO_2$ is its inability to solvate polar and ionic materials, a consequence of the molecule being nondipolar in the gas phase. This disadvantage can, however, be circumvented by using other polar compounds as cosolvents.[5,6] In particular, solutions of short chain alcohols in conjunction with $scCO_2$ are used widely in a variety of situations.[7,8] The addition of small amounts of cosolvents such as methanol or ethanol in $scCO_2$ can enhance the solubility of moderately polar compounds[9] and solid solutes.[10] This experimental observation has not yet been explored from a microscopic perspective. In this work, we attempt to study such a solvent mixture and provide molecular level details on the interactions between the solvent species.

The carbon atom in a $CO_2$ molecule is electron deficient, whereas the oxygen has two lone pairs of electrons. Thus, depending on its environment, $CO_2$ can act either as a Lewis acid or base,[11,12] conditions which can induce a dipole moment in $CO_2$.[13,14] In the former situation, the carbon atom behaves as an electron acceptor (partial charge transfer) from another molecule in the vicinity, whereas in the latter, the oxygen atom acts as an electron donor. The miscibility of cosolvents such as alcohols in $CO_2$ is linked closely to this aspect of the carbon dioxide molecule. The earliest quantitative data on the association between an alcohol and carbon dioxide was established by King and co-workers,[15,16] who determined large negative values for the cross second virial coefficient. However, alcohols are also known to aggregate in $scCO_2$ because of the stronger alcohol−alcohol[17] hydrogen bonding that can prevail over the weak association between alcohol and the solvent.[18,19] In a pioneering study, Smith and co-workers[20,21] carried out infrared spectroscopic measurements identifying such hydrogen bonds through a red shift in the stretching frequency ($\nu_1$) of the functional group relative to that in gas phase. However, static dielectric constant data[22] suggests a favorable interaction between ethanol and $CO_2$ under supercritical conditions. The variation in the dielectric constant upon mixing is found to be lesser than what is expected from an ideal, linear dependence on the mole fraction of ethanol. This can be understood as due to the disruption of the orientations of the linear ethanol molecules present in the electric field by $CO_2$ molecules. More recently, the interaction between ethanol and $CO_2$ in $scCO_2$ has been studied using vibrational spectroscopy that probes the O−D stretching in the alcohol as well as by ab initio calculations in the gas phase by Besnard and co-workers.[23,24] Han and co-workers[25] have studied the phase diagram of ethanol−$CO_2$ and $CO_2$−*n*-pentane mixtures. They have found that as the solvent pressure tends toward criticality, the local density of solvent molecules reduces, whereas the specific heat at constant volume increases.

There is astrophysical interest as well in the interaction between carbon dioxide and alcohols. Recent experiments carried out by the infrared space observatory have identified large amounts of $CO_2$ ice and methanol in protostellar environments.[26−29] The observed spectra have been interpreted based on vibrational spectroscopic experiments carried out on mixtures of methanol and $CO_2$ in the laboratory under different thermal conditions. These experiments were augmented by quantum chemical calculations on isolated complexes of the two

† Part of the special issue "Michael L. Klein Festschrift".

* Corresponding author. E-mail: bala@jncasr.ac.in.
‡ E-mail: moumita@jncasr.ac.in.

10.1021/jp053839f CCC: $33.50 
Published on Web 11/16/2005

molecules. The results show that although the bending mode of an isolated $CO_2$ molecule is doubly degenerate, it is split into two peaks in the complex. The lifting of the degeneracy in the associated complex is a consequence of $CO_2$ becoming nonlinear. The interaction is surmised to be of Lewis acid−base type wherein the electrons belonging to the interacting lone pair of the ethanol oxygen repel the oxygen atoms of the $CO_2$, causing it to bend. The intramolecular O−C−O angles have been calculated to be around 177°.[29] These results confirm the original gas-phase calculations of Jamroz et al.[30] on EDA complexes of $CO_2$.

Numerous computer simulation studies have been carried out to understand the properties of pristine $scCO_2$ as well as mixtures of $CO_2$ with other cosolvents/solutes. Most of these studies are simulations that employ an empirical potential[31,32] looking at various bulk properties of the solvent as well as its miscibility with solutes.[33,34] Recently, Stubbs and Siepmann have performed Monte Carlo calculations[34] of methanol−$CO_2$ mixtures with empirical potentials to examine its phase behavior and to study the formation of methanol aggregates in $scCO_2$. They observed the formation of hydrogen bonds between methanol molecules and, more importantly, the formation of a hydrogen bond between the hydroxyl hydrogen and the carbonyl oxygen. Configurations indicating the presence of EDA interactions between the carbonyl carbon and the alcohol oxygen were not reported. Earlier, we studied pure $scCO_2$ at 140 bar and 318.15 K using the Car−Parrinello molecular dynamics (CPMD) method.[14,35] Our calculations examined the evolution of the intramolecular bond angle in $CO_2$ and its deviation from linearity due to (i) thermal fluctuations and (ii) charge polarization from near-neighbor interactions. The polar attributes of carbon dioxide molecules in its interaction with other molecules have attracted much attention recently.[36] The ab initio MD (AIMD) work on $scCO_2$[14,35] has spurred researchers to find better interaction models for carbon dioxide,[37] a salient feature of which is the requirement of a flexible $CO_2$ in order to reproduce the experimental values of the dielectric constant as a function of pressure. It is thus crucial that such AIMD calculations, which inherently include flexibility and polarizability, are performed for cosolvent mixtures as well.

In this article, we study a mixture of carbon dioxide and ethanol under supercritical conditions. Our ab initio MD calculations employ only one ethanol molecule in a bath of 64 carbon dioxide molecules. Thus, our simulations cannot be used to study the phenomenon of alcohol aggregation in $scCO_2$, by construction. AIMD calculations of alcohol aggregates present in solvent would require very large system sizes and are beyond the scope of the current work. Thus, we limit this study to the investigation of microscopic interactions between alcohol and carbon dioxide molecules in $scCO_2$. Hence, despite its widespread use as a cosolvent in $scCO_2$, we call ethanol a "solute" within this paper. Calculations with larger mole fractions that include the effects of aggregation are planned to be performed in the future. The AIMD trajectory provides us with data on the structure around the ethanol, the dynamics of the molecules, and solute−solvent interactions. Inherently devoid of adjustable parameters, these calculations enable us to obtain insight into the microscopic organization of carbon dioxide molecules around ethanol. Anticipating our results, we find strong evidence, both in terms of structure and as well as in dynamics for Lewis acid−base type of interaction between $CO_2$ and ethanol in this bulk mixture. We follow this Introduction by providing details of the simulation and discuss the results of our analyses.

## 2. Simulation Details

Car−Parrinello MD simulations[38] were performed using the CPMD program,[39] whereas the classical MD calculations were carried out using the PINY_MD code.[40] The system consisted of one ethanol molecule soaked in a bath of 64 carbon dioxide molecules at a temperature of 318.15 K and a density of 0.699 $g/cm^3$ (system A). This thermodynamic condition is well above the critical point of carbon dioxide and that of the mixture as well. The mole fraction of ethanol in the solution is 0.0154. CPMD calculations were carried out within the density functional approximation. The exchange and correlation functionals were from the works of Becke,[41] and Lee, Yang, and Parr,[42] respectively, and thus fall into the category of generalized gradient approximated (GGA) functionals. Such functionals have been used in ab initio MD studies of proton transport in methanol earlier.[43] The electronic orbitals of valence electrons were expanded in a plane wave basis set with an energy cutoff of 70 Ry for the orbitals. Norm conserving pseudopotentials of the Troullier−Martins form[44] were employed for the treatment of the core electrons. To elucidate the influence of the ethanol molecule on the solvent structure, and to compare the structure of pure $scCO_2$ obtained using the BLYP functionals against our earlier LDA calculations, we have also carried out a bulk CPMD simulation of pure $scCO_2$ (32 $CO_2$ molecules, system B) at the same state point using the same procedures as described above, for a total run length of 10 ps with 2.9 ps for equilibration.

Two types of interactions are possible between ethanol and $CO_2$: (i) hydrogen bonding between the hydroxyl hydrogen of ethanol and the oxygen of $CO_2$ or (ii) a Lewis acid−Lewis base (LA-LB) interaction between the oxygen of ethanol and the carbon of $CO_2$.

These were investigated using gas-phase calculations on isolated dimers of $CO_2$ and an ethanol−$CO_2$ complex. Different initial configurations that varied in the locations of $CO_2$ with respect to ethanol were investigated. Calculations on the optimization of geometry of $CO_2$ clusters as well as the energy of dimerization using the functionals described above yielded results that are in good agreement with results reported in the literature using other methods. These are summarized and compared with data obtained from quantum chemical calculations in Table 1. The latter were carried out using the Gaussian[45] suite of programs with the 6-31++g* basis set, and electron correlations have been included according to density functional theory using Becke's three-parameter hybrid formalism[46] and Lee−Yang−Parr functionals[42] (B3LYP). These calculations show that the complex with a Lewis acid−base interaction between ethanol and $CO_2$ is energetically more favorable than the one with a hydrogen-bonded interaction between them. To aid further discussion, in Figure 1 we provide a schematic of atom nomenclature and parameters that are used to characterize the geometry of the EDA complex. For the study of the vibrational spectra of such clusters, CPMD trajectories of these systems present in a cubic box of edge length 13 Å were generated in the absence of periodic boundaries.

The 1:64 ethanol−$CO_2$ bulk system was equilibrated for around 40 ps using classical CHARMM all-atom potential model for ethanol[47] and the EPM2 model for $CO_2$ molecules.[48] Lorentz−Berthelot combination rules were employed for the cross interactions. The CPMD calculations were performed starting from the final configuration obtained from this classical MD simulation. All of the hydrogen atoms in ethanol were replaced by deuterium in order to be able to use a larger time step in CPMD calculations. The electronic wave functions were initially quenched to the Born−Oppenheimer surface. The

**TABLE 1: Geometry and Energetics of Optimized Clusters**

| species | angle | method | bond length (Å) | dimerization energy (kcal/mol) |
|---|---|---|---|---|
| $CO_2$ monomer | 180.0 (O═C═O) | CPMD | 1.176 | |
| | 180.0 (O═C═O) | Gaussian98 | 1.169 | |
| $CO_2$ dimer | 78.9 ($O_1-C_2-O_2$) | CPMD | ∼1.176 | −0.170 |
| (slipped parallel) | 100.9 ($C_2-O_2-C_1$) | | | |
| | 84.1 ($O_1-C_2-O_2$) | Gaussian98 | | |
| | 138.5 ($C_2-O_2-C_1$) | ref 29 | | |
| | | Gaussian98 | | −0.290 |
| | | ref 12 | | |
| ethanol−$CO_2$ | 123.1($\theta_1$) | CPMD | 2.833 ($O_e-C_C$) | −2.627 |
| EDA complex | 128.5($\theta_2$) | | | |
| | 120.9($\theta_1$) | Gaussian98 | 2.746 ($O_e-C_C$) | −2.720 |
| | 129.7($\theta_2$) | | | |
| | 114.7($\theta_1$) | Gaussian98 | 2.754 ($O_e-C_C$) | −2.417 |
| | | ref 23 | | |
| ethanol−$CO_2$ | 179.4 (O═C═O) | CPMD | 2.212 ($O_C-H_e$) | −0.840 |
| h-bonded complex | | | | |

[a] The subscripts 1 and 2 in the angle representation of the $CO_2$ dimer represent molecular indices.

fictitious dynamics of the electronic degrees of freedom was carried out with an electron mass of 500 au, which maintained the electrons at that surface. The equations of motion were integrated with a conservative time step of 4 au (around 0.096fs). Three-dimensional periodic boundary conditions consistent with a simple cubic box of edge length 18.843 Å were employed. In all, the system consisted of 201 atoms and 1044 valence electrons. Although the system contained only 64 $CO_2$ molecules, the box size is quite large when compared to a system of 64 molecules of, for example, liquid water under ambient conditions (a well studied case). The latter requires a cubic box of edge length of only 12.4 Å and possesses only 512 valence electrons. Thus, in comparison to a CPMD calculation of liquid water at the same system size, the current calculations are far more computationally demanding. Temperature control was achieved by the use of two Nosé−Hoover chain thermostats,[49] one for the ions and another for the electrons. The target kinetic energy for the electrons was set to 0.04 au, a value determined from preliminary NVE runs. The total run length was around 9.5 ps, which included a 1.85 ps trajectory devoted for equilibration. Because the system is in the supercritical phase, the diffusion coefficients of molecules are rather large,[35] and hence these run lengths are large enough to obtain meaningful properties. The fluctuation in the total energy was around one part in $10^5$.

Classical molecular dynamics simulations of this binary mixture at the same state point and composition as in the CPMD run were performed using the TraPPE-UA potential[50] for the sake of comparison. The TraPPE-UA potential is a united atom model for ethanol in which the $CH_3$ and $CH_2$ groups are replaced by pseudoatoms. In these runs, the system was equilibrated for 240 ps followed by a productive run of 360 ps during which the coordinates were stored at a regular interval of 40 fs. The nonbonded interactions were truncated at 9.25 Å. Note that the TraPPE-UA potential model prescribes an interaction cutoff of 14 Å, which could not be accommodated in the 1:64 classical MD run because of the smaller box size. To check if the decreased interaction cutoff leads to any changes in the intermolecular structure, we performed MD simulations of a large system, that of 1 ethanol molecule soaked in a bath of 240 $CO_2$ molecules. For these latter simulations, an interaction cutoff of 14 Å was employed. The radial distribution functions obtained for the smaller system were compared to those obtained from the 1:240 system. The only marked difference was that the first hump (which signifies hydrogen bonding) as well as the first peak in the $g(r)$ of the ethanol hydrogen to carbon dioxide's carbon was found to be marginally smaller in the larger system. Radial distribution functions (RDF) were calculated using a bin width of 0.2 Å.

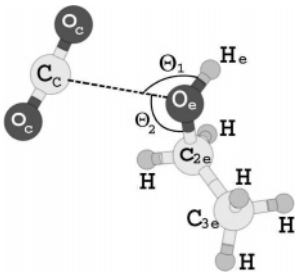


**Figure 1.** Nomenclature of atoms and angles for a typical EDA geometry of an ethanol−$CO_2$ complex.

In a seminal work, Stubbs and Siepmann[51] have provided a microscopic interpretation of the vibrational spectra of alcohol aggregates in a hydrocarbon solvent using ab initio MD methods. We draw inspiration from their work in the analyses of vibrational spectra of the bulk ethanol−$CO_2$ mixture. The vibrational density of states (VDOS) of $CO_2$ and ethanol were determined using regularized resolvent transformation (RRT)[52,51] of the velocity autocorrelation function of atoms. The RRT method enables one to obtain the spectrum at a higher resolution than a discrete Fourier transform. All of the spectra derived by RRT were compared to those obtained from a discrete Fourier transform to guard against numerical artifacts. Features in the VDOS spectra of the bulk 1:64 mixture have been interpreted by examining the VDOS of three clusters: (i) $CO_2$ monomer at 10 K, (ii) $CO_2$ dimer[12,53] in slipped parallel geometry at 10 K, and (iii) $CO_2$ and ethanol forming an EDA complex maintained at a temperature of 10 K. Each of these systems was studied by generating CPMD trajectories of duration around 8 ps.

## 3. Results and Discussion

**3.1. Structure.** *3.1.1. Isolated Molecules and Complexes.* The carbon atom in a $CO_2$ molecule can act as Lewis acid and can accept partial electronic charge. This charge could come from another molecule possessing a lone pair on any one of its atoms so that the pair of molecules could form a weak EDA complex. In the present study, we deal with the ethanol−$CO_2$ system where $CO_2$ can be treated as a Lewis acid (while forming an EDA complex with ethanol) as well as a Lewis base while

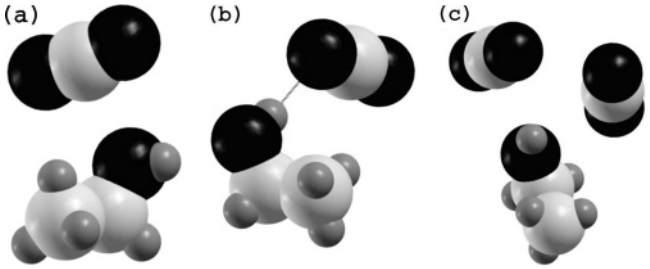


**Figure 2.** Snapshots of cluster configurations. (a) Ethanol−$CO_2$ EDA complex obtained by geometry optimization within CPMD. (b) Ethanol−$CO_2$ hydrogen-bonded configuration obtained from geometry optimization within CPMD. (c) An EDA complex containing two $CO_2$ molecules and one ethanol molecule, obtained as a snapshot from the CPMD trajectory of the bulk ethanol−$CO_2$ mixture. Oxygen atoms are shown in black, carbon atoms are in white, and hydrogen atoms are in gray.

forming a hydrogen-bonded complex with ethanol. Even in the absence of a solute, such LA−LB interactions are possible between $CO_2$ molecules. The optimized configurations of isolated ethanol−$CO_2$ complexes obtained from CPMD are exhibited in Figure 2. In Table 1, we compare the geometry and energetics of these clusters with earlier investigations and that obtained from our Gaussian98 calculations. Although the binding energy and $O_e-C_C$ distance for the EDA complex are in good agreement with the work of Tassaing et al.,[23] angle $\theta_1$ is slightly different. This difference may arise because of the different basis sets used for the optimization. It can be noticed that in the CPMD method, the EDA complex with ethanol is energetically more stable than the hydrogen-bonded one. Note that the difference in the binding energies between the EDA and hydrogen-bonded states are accessible to thermal fluctuations at and near ambient conditions. However rare, it is also possible for two carbon dioxide molecules to be simultaneously proximal to the ethanol oxygen in an EDA-like geometry because oxygen possesses two lone pairs of electrons. A snapshot of an occurrence of such a kind observed in the bulk ethanol−$CO_2$ system is shown in Figure 2c. We isolated such a complex of one ethanol molecule associated with two $CO_2$ molecules from the bulk system and used it as a starting configuration for geometry optimization. This run did not converge, and we noticed large separations between the molecules of the complex at the end of the run. Hence, it is possible that such a double EDA complex could be stabilized by entropic factors alone.

*3.1.2. Bulk Calculations.* 3.1.2.1. Pair Correlation Functions. The purpose of this work is to provide molecular-level insight into the solvent structure around the solute. The radial distribution function is an important tool for investigating the arrangement of near-neighbor molecules around a central one. Figure 3 compares the partial intermolecular RDFs between $CO_2$ molecules in the solution, obtained from both ab initio and classical MD calculations. All of the RDF curves are observed to nearly reach their uncorrelated value of unity within half of a boxlength, which indicates that the system size studied here is probably large enough for proper simulation of the fluid phase. The first minima of $g_{CC}(r)$ (Figure 3a) are observed at 6.15 Å and 5.90 Å for the CPMD and MD calculations, with corresponding coordination numbers of 9.5 and 8.4, respectively. Figure 3b shows the $g_{CO}(r)$. Here too we observe a higher population of oxygen atoms around carbon in CPMD than in MD simulations. In Figure 3c, we compare the CO pair correlation functions obtained from systems A and B. The two curves are nearly identical, which indicates that the influence of ethanol on the solvent structure is negligible in its present

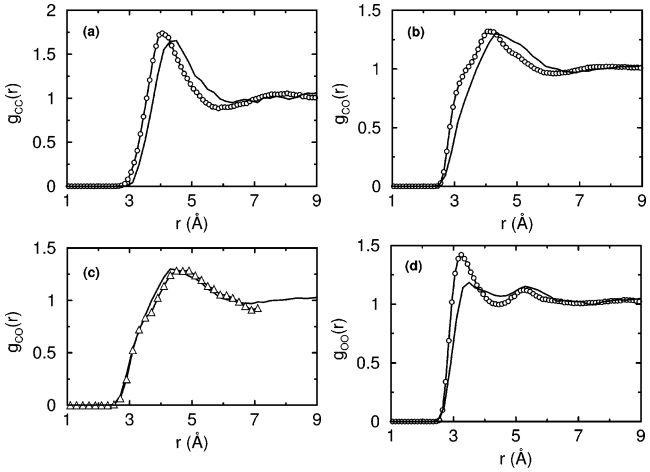


**Figure 3.** $CO_2-CO_2$ intermolecular pair correlation functions obtained from the 1:64 system. Solid lines represent CPMD results, lines with open circles represent classical MD results, and the line with open triangles in (c) represents the result from system B.

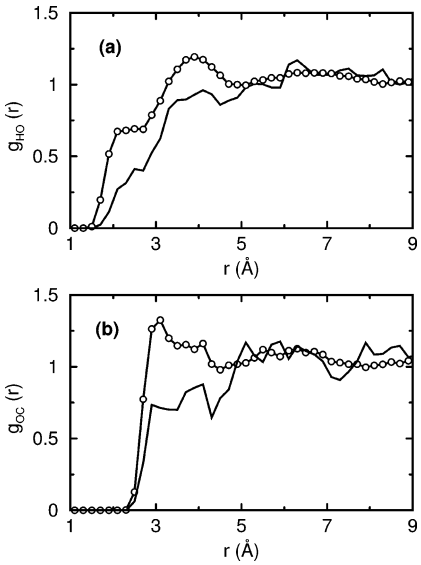


**Figure 4.** Ethanol−$CO_2$ intermolecular pair correlation functions obtained from the 1:64 system. Solid lines represent CPMD results and lines with open circles represent classical MD results.

concentration. It also indicates that a system size of 32 molecules is large enough to capture the crucial features of intermolecular structure in $scCO_2$ at this state point. The hump at 3.2 Å that was observed in our earlier work on pure $scCO_2$[35] is present only as a weak shoulder in the current ethanol−$scCO_2$ system. It thus appears that the LDA calculation generates a fluid that is more structured than the current simulations that employ the BLYP functionals. Results from the classical simulations using empirical potentials lie between the data obtained from LDA- and BLYP-based simulations. Similar differences between LDA and GGA functionals have been well documented in the literature, specifically for the case of liquid water.[54] The same trend has been observed in $g_{OO}(r)$ (Figure 3d), where the first maxima is less peaked than that in neat $CO_2$.

The distribution of $CO_2$ molecules around a central ethanol molecule has been investigated by two partial radial distribution functions shown in Figure 4. The first hump at around 2.5 Å in the RDF for $CO_2$'s oxygen around a central hydroxyl hydrogen of ethanol obtained from both CPMD and classical MD data, indicates a hydrogen-bonded interaction between these two species (Figure 4a). The same has been observed in the Monte

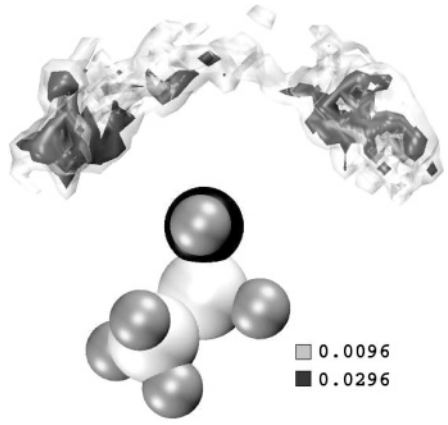


**Figure 5.** Probability density map for the location of $CO_2$'s carbon atom within a distance of 4.3 Å from $O_e$, obtained from CPMD data of the bulk mixture. Gray and black regions represent low and high probability, respectively. Oxygen atoms are shown in black, carbon atoms are in white, and hydrogen atoms are in gray. The OH vector of the hydroxyl group points along the normal to the paper. The density values are in units of $Å^{-3}$.

Carlo work of Stubbs and Siepmann[34] in the methanol−$CO_2$ system. However, hydrogen bonding between the species is found to be much weaker in the corresponding CPMD results. The coordination number for the two $g(r)$'s integrated up to the standard hydrogen bond length of 2.5 Å is around 0.28 and 0.64, respectively, obtained from CPMD and MD calculations. It may be pertinent to confirm the relative weakening of the hydrogen-bonded configuration in CPMD by studies using other exchange-correlation functionals. If the current results are validated, then the interaction potential for classical MD may have to be refined so as to reproduce the ab initio results. The radial distribution function of $C_C$ with respect to $O_e$ (Figure 4b) is peaked at around 4.1 Å in CPMD and at 3 Å in MD simulations. The first minimum of this $g(r)$ is at 4.3 Å. The coordination number up to the first minimum is around 2.0 and 3.0 from CPMD and classical MD simulations, respectively. We choose this distance as the upper limit for $C_C-O_e$ separation in the formation of EDA complexes in bulk.

3.1.2.2. Characterization of Electron Donor−Acceptor and Hydrogen-Bonded Complexes. An idea of the geometry of the EDA complex can be obtained by studying the atomic probability density map (also called the spatial distribution function). Figure 5 shows the probability distribution for the location of carbonyl carbon ($C_c$) situated within 4.3 Å of the oxygen ($O_e$) atom of ethanol, with the data averaged over the full trajectory. The two shades represent different probabilities of finding $C_c$ around the central $O_e$. The two distinct lobes of high probability point to the directional nature of the EDA interaction between the lone pair of ethanol's oxygen with $CO_2$'s carbon. Note that the lobes appear to be along the direction of the central oxygen's lone pairs.

Hydrogen bonds are often identified in molecular simulations using a set of geometric criteria that limit the oxygen−oxygen distance to 3.5 Å, the donor hydrogen−oxygen distance to 2.5 Å, and the oxygen−oxygen−donor hydrogen angle to be greater than 140°.[34,55] Because the EDA interactions reported here are also quite directional just as hydrogen bonds are, we could develop a similar set of conditions. As mentioned earlier, we choose a 4.3-Å cutoff for the distance between the ethanol oxygen and carbonyl carbon. This distance corresponds to the first minimum in the corresponding pair correlation function. In addition, two angle conditions need to be employed because the EDA interaction is directional, a part of the lone pair

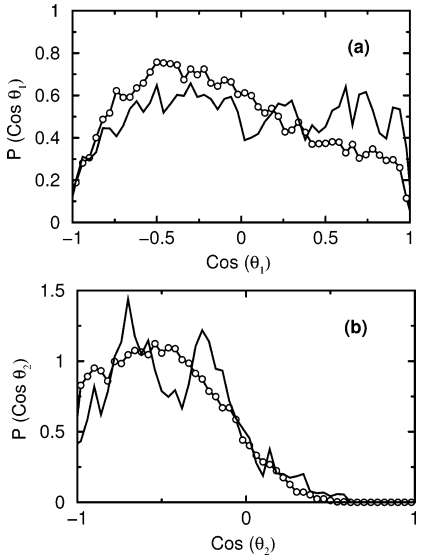


**Figure 6.** Probability distributions for angles $\theta_1$ and $\theta_2$ obtained for $C_c-O_e$ pairs present within a distance of 4.3 Å. Solid lines represent CPMD results, and lines with open circles represent classical MD results.

electrons of the ethanol oxygen being donated to the acidic carbon of $CO_2$. In the following, we provide a rationale for the choice of these angle conditions by studying their probability distributions.

The probability distribution of cosines of $C_c-O_e-H_e$ ($\theta_1$) and $C_c-O_e-C_{2e}$ ($\theta_2$) angles for carbon dioxide molecules that satisfy the $C_c-O_e$ distance cutoff (of 4.3 Å) are shown in Figure 6. The distribution for $\theta_1$ exhibits a rather weak preference for the tetrahedral angle and that for $\theta_2$ shows a peak at a cosine value of −0.33. Thus, carbon dioxide molecules are seen to have a preferred orientation with respect to the oxygen atom of the ethanol molecule, a consequence of the Lewis acid−base interaction between them.

To arrive at reasonable angular limits to define the EDA complex, we have analyzed the $O_e-C_c$ pair correlation functions with different angular ranges of $\theta_1$ and $\theta_2$. We have obtained these functions for $C_c$ atoms, which fall within a given angular range in both $\theta_1$ and $\theta_2$, around the ethanol molecule. The volume element required for normalization of the function was estimated numerically by generating uniform random numbers that fall within the spherical shell of the required radius, a procedure akin to the numerical calculation of the value of $\pi$ using an elementary Monte Carlo procedure.[56] Pair correlation functions of those $C_c$ atoms that do not satisfy the two angular conditions were also obtained for purposes of reference. These are compared in Figure 7 for three different angular limits placed on $\theta_1$ and $\theta_2$. Note the presence of sharp peaks in the functions that satisfy the angular conditions relative to the ones that do not satisfy them. This behavior shows the presence of a preferred window of angle in the formation of the EDA complex. The intensity of the first peak in the $g(r)$ that satisfies the angular condition, upon increasing the angular limits, is gradual and not dramatic. This implies that the EDA interaction is only weakly angle-dependent (in these ranges of angles). In the following discussion, we choose the range of $\theta_1$ and $\theta_2$ angles for the existence of a LA−LB complex to be between 90° and 130°. The results to be discussed on the concentration of EDA complex in bulk and its properties do depend on this choice. We have provided results on sensible alternate choices of these angular limits as well, to provide a perspective.

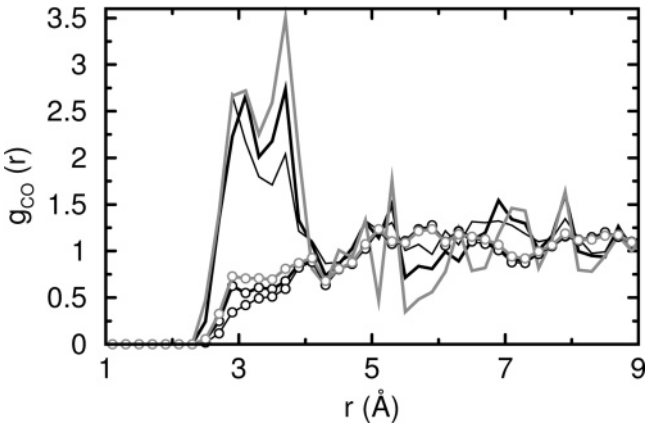


**Figure 7.** Radial distribution functions of the $O_e-C_c$ pair obtained from the CPMD calculation. Solid lines represent $g_{CO}(r)$ within the angular range defining the EDA complex, and lines with open circles represent outside the angular range. $90° \le \theta_1, \theta_2 \le 130°$ (thick black), $80° \le \theta_1, \theta_2 \le 140°$ (thin black), and $100° \le \theta_1, \theta_2 \le 120°$ (gray).

Armed with this set of criteria for defining the EDA complex (and a similar well-established one to define the hydrogen bond), we proceed to calculate the ratio of occurrence of these types of configurations in the ethanol−$CO_2$ mixture. Within our trajectory of length 7.7 ps, the signatures of the EDA complex were observed in several segments together spanning a length of 3.0 ps, whereas the hydrogen-bonded configuration was observed for a total duration of around 0.6 ps. In the remaining duration of the trajectory, the ethanol molecule did not satisfy either the EDA criteria or the hydrogen-bond criteria. The EDA interaction is thus favored even in the bulk phase at finite temperature, consistent with our observations on the energetics of these complexes in the gas phase. We can assume that these two states exist in a dynamical equilibrium along with another state in which the ethanol and the carbon dioxide are not associated through either a hydrogen bond or an EDA-type arrangement. In the rest of the discussion, we ignore the "disassociated" state. The equilibrium constant, $K$, between the EDA arrangement and the hydrogen-bonded complex is equal to the ratio of their concentrations and thus of the ratio of the durations that they were observed for. $K$ is related to the free-energy difference between these two states, $\Delta A$ as

$$\Delta A = -RT \ln K \qquad (1)$$

where $R$ is the universal gas constant. $\Delta A$ is determined to be −0.88 kcal/mol, for the choice of angular domain of 40° (with limits on $\theta_1$ and $\theta_2$ being 90° and 130°). This free-energy difference changes to −0.24 kcal/mol and −1.36 kcal/mol for the angle choices of 100−120° and 80−140°, respectively. Note that the energy difference between the EDA and hydrogen-bonded complex in the gas phase is −1.79 kcal/mol. Thus, irrespective of the choice of the angle limits, relative to the hydrogen-bonded moiety, the EDA complex is more stable in the gas phase than in the bulk system because the free-energy difference is found to be smaller than the energy difference between the gas-phase (zero Kelvin) complexes.

Earlier investigations[29,30] on the ethanol−$CO_2$ complex have shown that the $CO_2$ molecules prefer two possible orientations with respect to the ethanol: "parallel" (or horizontal) and "perpendicular" (or vertical) arrangements. In the parallel orientation, the plane of $CO_2$ lies parallel to the $H_e-O_e-C_{2e}$ plane of ethanol, whereas it is perpendicular in the perpendicular orientation. On the basis of quantum chemical calculations of isolated EDA complexes, the parallel configuration has been reported to be more stable than the perpendicular one.[29] In Figure 8, we show the probability distribution of the cosine of the angle ($\phi$) between the $H_e-O_e-C_{2e}$ plane of ethanol and the plane of $CO_2$ during instances in the CPMD trajectory when the EDA complex is formed. Such distributions obtained from both CPMD and classical MD exhibit peaks at $\cos\phi = \pm 1$, which is consistent with the gas phase work of Dartois and coworkers.[29]

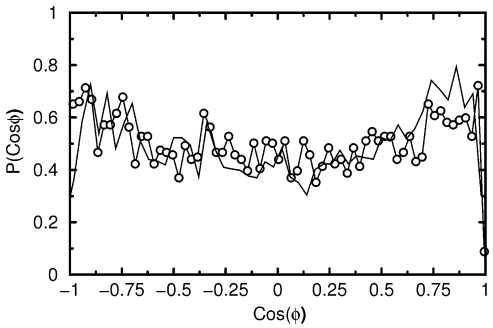


**Figure 8.** Probability distribution of $\cos(\phi)$, where $\phi$ represents the angle between the instantaneous $O_C-C_C-O_C$ and $C_{2e}-O_e-H_e$ planes. The solid line represents CPMD results, and the line with open circles represents the classical MD result.

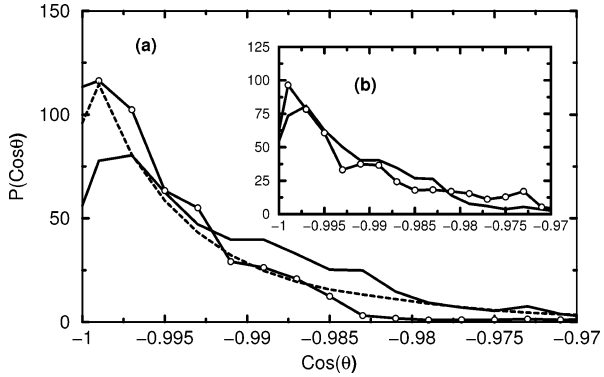


**Figure 9.** Probability distribution for the intramolecular $O_C-C_C-O_C$ angle of $CO_2$ molecules for "free" $CO_2$ (dashed line), $CO_2$ while forming an EDA complex with ethanol (solid line), and $CO_2$ while forming a hydrogen bond with ethanol (open circles). Inset: The same for $CO_2$ while forming an EDA complex with ethanol (solid line, same as in the main body), and two $CO_2$ molecules simultaneously forming an EDA complex with ethanol (line with open circles). The data are obtained from the CPMD run of the bulk 1:64 mixture.

**Linearity of $CO_2$.** As discussed in the Introduction, interactions with ethanol can influence the carbon dioxide molecule to assume a nonlinear geometry. Our earlier work[14,35] showed that instantaneous nonlinear $CO_2$ configurations are possible at high enough pressures because of interactions between $CO_2$ molecules themselves. This could be caused by thermal fluctuations as well as by instantaneous anisotropic distributions of neighbors in the first coordination shell. The latter would polarize the electron density of a central $CO_2$ molecule, leading to deviations from a linear geometry, as well as imparting a molecular dipole moment to the instantaneous configuration.[14] It would thus be interesting to investigate the geometry of the carbon dioxide molecule(s) that interact favorably with ethanol. We provide results on the intramolecular $O_C-C_C-O_C$ angle of $CO_2$ in various contexts in Figure 9. The probability distribution for the instantaneous value of the intramolecular angle of $CO_2$ molecules that satisfy the conditions of the hydrogen bond (with ethanol) is marginally narrower than that for molecules interacting with ethanol via the EDA interaction. The latter forces the $CO_2$ molecule to adopt a more bent geometry. Note that, a value

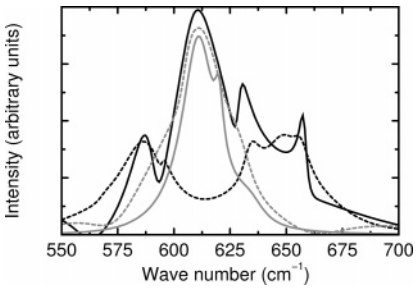


**Figure 10.** Power spectrum of $CO_2$ molecules in the bending region. Total bending mode in the bulk mixture (black solid line), In-plane (black dashed line) and out-of-plane (gray solid line) modes in bulk, and for the $CO_2$ monomer (gray dashed line) at 318.15 K.

of −0.985 in cosine of the angle implies that the $O_C-C_C-O_C$ angle is 170°, a deviation of 10° from linearity. This is significant and may not be entirely captured in zero Kelvin quantum chemical calculations of isolated ethanol−$CO_2$ dimers. The distribution for molecules that neither form a hydrogen bond with ethanol nor interact via the EDA interaction, that is, *free $CO_2$* is also shown. This distribution is again narrower relative to the one for EDA interaction. As discussed earlier, it is also possible for two $CO_2$ molecules to simultaneously interact with the two lone pair electrons on the oxygen of the ethanol molecule. Such configurations are, however, rare. In the inset to Figure 9, we show the distribution of the intramolecular $O_C-C_C-O_C$ angle for such $CO_2$ molecules. This distribution appears to be quite similar to that for a single EDA complex, although slightly narrower.

**3.2. Vibrational Dynamics.** Experimentally, ethanol−$CO_2$ interactions in the supercritical phase have been explored by examining the O−H stretching mode in ethanol. This mode is known to undergo a red shift in frequency relative to its value in gas phase.[20] Besnard and co-workers[24] have observed a red shift in the OD stretching frequency, $\nu_{OD}$, as a function of increasing pressure for deuterated ethanol present in $scCO_2$. The $\nu_{OD}$ stretching mode of the ethanol monomer was observed to be at 2700 cm$^{-1}$ at 120 °C. The spectral shift with increase in pressure was attributed to an attractive interaction between ethanol and carbon dioxide. Early spectroscopic experiments focused on the aggregation of methanol molecules in $scCO_2$ at high concentrations.[21] Thus, the shifting of the OH stretching mode to lower frequencies in these samples could also be due to the formation of hydrogen bonds between alcohol molecules. Here we study the effect of the interactions between the single alcohol molecule and $CO_2$ in the supercritical phase on their vibrational spectra. First we discuss the spectral features associated with the bending mode of carbon dioxide and follow it up with those observed for the stretching of the hydroxyl group of d-ethanol.

*3.2.1. $CO_2$ in Bulk.* Figure 10 compares the $\nu_2$ bending mode of $CO_2$ in the bulk mixture and in the gas phase. It can be observed clearly that both curves are peaked at 613 cm$^{-1}$. $CO_2$ in bulk shows an additional peak at 633 cm$^{-1}$ and a shoulder at 589 cm$^{-1}$. In contrast, the isolated $CO_2$ monomer does not show any split in the bending mode, consistent with its $D_{\infty h}$ symmetry. Thus, the $CO_2$ bending mode is doubly degenerate under isolated conditions. This degeneracy gets lifted because of near-neighbor interactions with other molecules, as will be discussed in sections 3.2.2. and 3.2.3.

A recent study on Raman spectroscopy of $CO_2$−acetone and $CO_2$−ethanol binary mixtures[57] shows that the removal of degeneracy in the bending mode of $CO_2$ is due to charge-transfer interactions between the two species. A similar kind of spectral behavior of $CO_2$ has been observed by Kazarian et al[58] for molecules of $CO_2$ gas interacting with the carbonyl side group of poly(methyl methacrylate) (PMMA), and by Dartois et al[28] at low temperatures in $CO_2$−methanol mixtures. The PMMA−$CO_2$ work shows a change in the behavior of the bending mode of $CO_2$ under three different conditions: when $CO_2$ is in gas phase, when the PMMA film is impregnated with $CO_2$, and after removal of gaseous $CO_2$ from the system. For the second case, three peaks in this mode were assigned to free $CO_2$ (at 667 cm$^{-1}$), in-plane mode (654 cm$^{-1}$), and out-of-plane (662 cm$^{-1}$) mode, the last two arising because of the EDA interaction between the polymer and the $CO_2$ molecule. Our calculations agree with experiments on the fact that multiple peaks are observed for the $CO_2$ part of the infrared spectrum.[59] However, the calculations consistently predict lower values for these peak positions relative to the experiments. This red shift could probably arise because of the nature of the exchange and correlation approximations as well as the lower value of the energy cutoff employed here. Determination of exact frequencies of vibration would probably require calculations with a 120 Ry cutoff, which is beyond the scope of this work. In addition, the state point of our calculations is 45 °C and 140 bar, whereas the experimental data is at 40 °C and 400 bar.

We delve further into the microscopic origin of these multiple peaks. To accomplish this task, we have decomposed the total $CO_2$ bending mode into two parts: in-plane and out-of-plane modes, which are defined with respect to the instantaneous $O_C-C_C-O_C$ plane of each $CO_2$ molecule. The in-plane bending mode of $CO_2$ in the ethanol−$CO_2$ supercritical fluid shows two distinct peaks at around 589 cm$^{-1}$ (present as a shoulder in the total $CO_2$ spectra) and at 636 cm$^{-1}$. The out-of-plane mode is peaked at 613 cm$^{-1}$, which corresponds to the fundamental $\nu_2$ mode of $CO_2$ in the ethanol−$CO_2$ mixture. Experimental studies on mixtures of $CO_2$ and Lewis bases using FTIR spectroscopy reveals the splitting of the $CO_2$ bending mode with red shifted in-plane and blue shifted out-of-plane bending modes where the definition of plane was different[60] from ours.

We can infer two reasons for the splitting of the in-plane bending mode of $CO_2$. These are (i) the formation of an EDA complex between $CO_2$ and ethanol and (ii) the formation of an EDA-like complex between $CO_2$ molecules themselves. To understand this further, we have compared the $CO_2$ spectrum of the bulk ethanol−$CO_2$ solution with those obtained from a ethanol−$CO_2$ EDA cluster and a $CO_2$ dimer cluster. The latter spectra are obtained once again from individual MD runs at a low temperature of 10 K, each of length around 8 ps. The low temperature was employed in order to prevent the EDA complex from disintegrating as well as to obtain sharp spectral features.

*3.2.2. Isolated Ethanol−$CO_2$ EDA Complex.* The spectrum for the ethanol−$CO_2$ EDA complex shows two clear peaks (Figure 11), one at 604 cm$^{-1}$ and another at 618 cm$^{-1}$. Importantly, the spectrum has no feature at 612 cm$^{-1}$, the frequency of vibration observed for an isolated $CO_2$ molecule. In the isolated ethanol−$CO_2$ EDA complex, the in-plane bending mode is present at 604 cm$^{-1}$, and the out-of-plane mode is at 618 cm$^{-1}$.

*3.2.3. Isolated $CO_2$−$CO_2$ EDA Complex.* We now examine the vibrational spectrum of a dimer cluster of $CO_2$ in Figure 12. Here, the in-plane modes are present at 592, 611, and 625 cm$^{-1}$, whereas the out-of-plane bending mode is present at 614 cm$^{-1}$ with a small hump at 596 cm$^{-1}$. The in-plane bending mode of $CO_2$ in the dimer and in bulk exhibit similar behavior, leaving aside the thermal broadening in the bulk data. It is thus confirmed that the lone pair on the donating oxygen atom of a

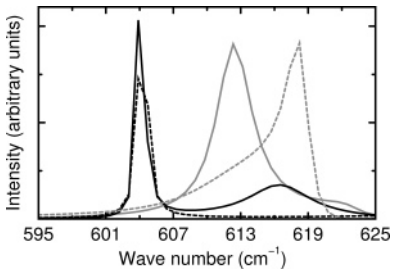


**Figure 11.** $\nu_2$ bending mode of the ethanol−$CO_2$ EDA complex and of $CO_2$ monomer at 10 K obtained as power spectrum from CPMD runs. Total EDA bending mode (black solid line), in-plane (black dashed line) and out-of-plane (gray dashed line) modes, and for the $CO_2$ monomer (gray solid line).

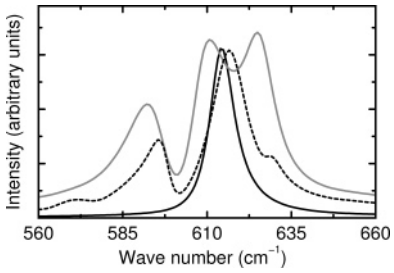


**Figure 12.** $\nu_2$ bending mode of $CO_2$ dimer at 10 K. Total bending mode (black solid line), in-plane (gray solid line), and out-of-plane (black dashed line) modes.

$CO_2$ molecule interacts with the carbon atom of an acceptor $CO_2$ molecule, thus giving rise to the distorted T-shaped EDA complex.

From these spectral analyses, one can conclude that the characters of Lewis acid−base interaction between the two categories of EDA complexes are likely to be different. In the $CO_2$−$CO_2$ EDA complex, the out-of-plane mode remains unaffected by LA−LB interaction, and in the ethanol−$CO_2$ EDA complex it gets shifted to 618 $cm^{-1}$.

Thus, the $\nu_2$ mode of the $CO_2$ dimer exhibits a close resemblance to that in bulk. This is to be expected because the concentration of ethanol in our solution is small. In conclusion, one can argue that the major reason for the splitting in the bending mode of $CO_2$ in the 1:64 system is due to a $CO_2$−$CO_2$ LA−LB interaction, and the minor contribution is the Lewis acid−base interaction between ethanol and $CO_2$.

*3.2.4. Ethanol Spectrum.* The vibrational density of states of d-ethanol in this 1:64 bulk solution as well as in the isolated configuration are shown in Figure 13. The inset shows the same in the region of the OD stretching in expanded scale. The stretching frequency is observed at 2536 $cm^{-1}$ for the isolated ethanol, which is found to be shifted to around 2400 $cm^{-1}$ in 1:64 bulk mixture. This is to be compared to the experimental value of 2690 $cm^{-1}$.[24] Note that the concentration of ethanol in the recent experiments of Besnard and co-workers[24] is $6 \times 10^{-3}$ mol·$L^{-1}$, whereas it is 0.248 mol·$L^{-1}$ in our simulations. Also, the experiments were conducted at a temperature of 120 °C, whereas our simulations were performed at 45 °C. These differences in the state conditions of the sample could also explain the difference in OD stretching frequency between our calculations and experiment, apart from the DFT approximation. However, crucially we agree with experiments in the observation of a red shift in the OD stretching frequency upon complexation.

## 4. Conclusions

We have carried out Car−Parrinello molecular dynamics simulation studies of a system containing one ethanol molecule soaked in 64 molecules of carbon dioxide under supercritical conditions. The current calculations improve upon our earlier work on pure $scCO_2$ in two aspects: (i) the system size is twice as large and (ii) the use of exchange and correlation functionals that include correction terms in the gradient of the electronic density in lieu of the local density approximation. The increase in system size is expected to address issues related to the absence of a clear second neighbor shell in our previous work, whereas the gradient corrections enhances the accuracy of weak interactions in this solvent. The focus of this work is to shed light on microscopic interactions prevailing in a mixture of carbon dioxide and ethanol. The latter is used widely as a cosolvent to enhance the solubility of polar solutes in $scCO_2$. The important observations from our study are as follows: Carbon dioxide and ethanol can interact favorably with each other either by forming an electron donor−acceptor complex or through the formation of a hydrogen bond. Both interactions are directional. In the EDA complex, the oxygen atom of ethanol acts as an electron donor and the carbon atom of $CO_2$ acts as an acceptor. Our observations on both isolated (gas-phase) complexes as well as on the bulk mixture at finite temperature show that the EDA interaction is favored more than hydrogen bonding. The EDA complex is thus the preferred one both in terms of potential energy as well as in free-energy terms. The ratio of their occurrence in bulk solution is around 4:1. The dependence of this ratio as a function of increasing ethanol concentration needs to be explored.

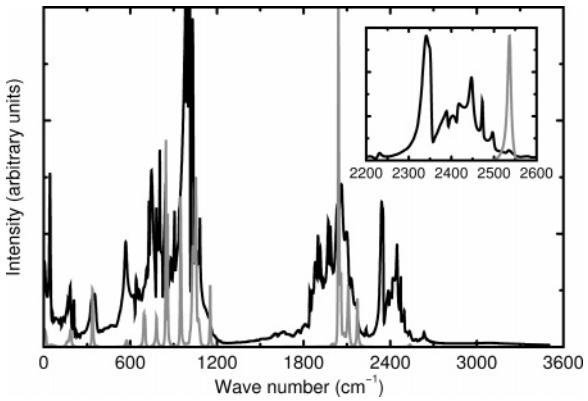


**Figure 13.** Total vibrational spectrum of d-ethanol in the bulk mixture at 318.15 K (black line) and as a monomer in gas phase (gray line) at 10 K. The inset shows the vibrational spectra of the hydroxyl oxygen of the ethanol molecule for both cases in the OD stretching region. In the inset, the intensity of the monomer spectrum has been scaled by an order of magnitude for the sake of comparison.

The directionality of the EDA interaction is such that the preferred orientation of the carbon atom of an approaching $CO_2$ molecule is along the direction of the lone pair of electrons on the ethanol oxygen. This Lewis acid−base interaction leads to a considerable deviation from linearity of the carbon dioxide molecule. We have also found evidence for the occurrence of two $CO_2$ molecules interacting simultaneously with ethanol via an LA−LB type of arrangement. However, their population is relatively rare, and only 10% of EDA complexes are of such a variety. The nonlinearity in the backbone angle of $CO_2$ lifts the degeneracy of its $\nu_2$ bending mode. Thus, in this region of frequency, several spectral features are observed. These have been interpreted through our simulations on isolated complexes as well as by projection of atomic velocities on the $O_C$−$C_C$−$O_C$ plane, as due to in-plane and out-of-plane bending vibrations. The distinction between these bending vibrations are caused by the association of a central $CO_2$ molecule with other carbon dioxide molecules or with ethanol. The current calculations have

provided a microscopic perspective to ethanol−$CO_2$ interactions in the bulk supercritical phase. Further simulations on higher mole fractions of ethanol need to be performed in order to complete this understanding. It may also be pertinent to employ other exchange-correlation functionals such as PBE[61] to verify and augment the current results. Modeling of industrially relevant solutes such as caffeine in such solvent mixtures is also being pursued.

**Acknowledgment.** S.B. gratefully acknowledges Professor Mike Klein for his mentorship, generosity, and for insightful discussions on several scientific topics. Helpful discussions with Professor J. M. Stubbs and Professor M. Vladimir on the RRT method are greatly appreciated. We also thank the latter for providing us the program to perform the RRT calculations. We thank Dr. N. Arul Murugan and Mr. Ayan Dutta for helpful suggestions regarding geometry optimization of different molecular clusters using Gaussian98. The research reported here was supported in part by grants from the Council of Scientific and Industrial Research (CSIR), India.

## References and Notes

(1) Leitner, W. *Nature* **2000**, *405*, 129−130.
(2) Poliakoff, M.; King, P. *Nature* **2001**, *412*, 125.
(3) Wells, S. L.; DeSimone, J. *Angew. Chem., Int. Ed.* **2001**, *40*, 519−527.
(4) DeSimone, J. M. *Science* **2002**, *297*, 799−803.
(5) Zhang, X.; Han, B.; Hou, Z.; Zhang, J.; Liu, Z.; Jiang, T.; He, J.; Li, H. *Chem.—Eur. J.* **2002**, *8*, 5107−5111.
(6) Tassaing, T.; Lalanne, P.; Rey, S.; Cansell, F.; Besnard, M. *Ind. Eng. Chem. Res.* **2000**, *39*, 4470−4475.
(7) Tomasko, D. L.; Knutson, B. L.; Pouillot, F.; Liotta, C. L.; Eckert, C. A. *J. Phys. Chem.* **1993**, *97*, 11823−11834.
(8) Lu, J.; Han, B.; Yan, H. *Phys. Chem. Chem. Phys.* **1999**, *1*, 3269−3276.
(9) Jin, J.; Zhong, C.; Zhang, Z.; Li, Y. *Fluid Phase Equilib.* **2004**, *226*, 9−13.
(10) Li, Q.; Zhang, Z.; Zhong, C.; Liu, Y.; Zhou, Q. *Fluid Phase Equilib.* **2003**, *207*, 183−192.
(11) Bell, P. W.; Thote, A. J.; Park, Y.; Gupta, R. B.; Roberts, C. B. *Ind. Eng. Chem. Res.* **2003**, *42*, 6280−6289.
(12) Raveendran, P.; Wallen, S. L. *J. Am. Chem. Soc.* **2002**, *124*, 12590−12599.
(13) Amos, R. D.; Buckingham, A. D.; Williams, J. H. *Mol. Phys.* **1980**, *39*, 1519−1526.
(14) Saharay, M.; Balasubramanian, S. *ChemPhysChem.* **2004**, *5*, 1442−1445.
(15) Hemmaplardh, B.; King, A. D. *J. Phys. Chem.* **1972**, *76*, 2170−2175.
(16) Gupta, S. K.; Lesslie, R. D.; King, A. D. *J. Phys. Chem.* **1973**, *77*, 2011−2015.
(17) Taylor, C. M. V.; Bai, S.; Mayne, C. L.; Grant, D. M. *J. Phys. Chem. B* **1997**, *101*, 5652−5658.
(18) Kanakubo, M.; Aizawa, T.; Kawakami, T.; Sato, O.; Ikushima, Y.; Hatakeda, K.; Saito, N. *J. Phys. Chem. B* **2000**, *104*, 2749−2758.
(19) Yamamoto, M.; Iwai, Y.; Nakajima, T.; Arai, Y. *J. Phys. Chem. A* **1999**, *103*, 3525−3529.
(20) Yee, G. G.; Fulton, J. L.; Smith, R. D. *J. Phys. Chem.* **1992**, *96*, 6172−6181.
(21) Fulton, J. L.; Yee, G. G.; Smith, R. D. *J. Am. Chem. Soc.* **1991**, *113*, 8327−8334.
(22) Wesch, A.; Dahmen, N.; Ebert, K. H. *Ber. Bunsen-Ges. Phys. Chem.* **1996**, *100*, 1368−1371.
(23) Danten, Y.; Tassaing, T.; Besnard, M. *J. Phys. Chem. A* **2002**, *106*, 11831−11840.
(24) Lalanne, P.; Tassaing, T.; Danten, Y.; Cansell, F.; Tucker, S. C.; Besnard, M. *J. Phys. Chem. A* **2004**, *108*, 2617−2624.
(25) Li, H.; Zhang, X.; Han, B.; Liu, J.; He, J.; Liu, Z. *Chem.—Eur. J.* **2002**, *8*, 451−456.
(26) Ehrenfreund, P.; Boogert, A. C. A.; Gerakines, P. A.; Tielens, A. G. G. M.; Dishoeck, E. F. *Astron. Astrophys.***1997**, *328*, 649−669.
(27) Ehrenfreund, P.; Dartois, E.; Demyk, K.; d'Hendecourt, L. *Astron. Astrophys.* **1998**, *339*, L17−L20.
(28) Dartois, E.; Demyk, K.; d'Hendecourt, L.; Ehrenfreund, P. *Astron. Astrophys.* **1999**, *351*, 1066−1074.
(29) Koltz, A.; Ward, T.; Dartois, E. *Astron. Astrophys.* **2004**, *416*, 801−810.
(30) Jamroz, M. H.; Dobrowolski, J. C.; Bajdor, K.; Borowiak, M. A. *J. Mol. Struct.* **1995**, *349*, 9−12.
(31) Rocha, S. R. P.; Johnston, K. P.; Westacott, R. E.; Rossky, P. J. *J. Phys. Chem. B* **2001**, *105*, 12092−12104.
(32) Zhang, Z.; Duan, Z. *J. Chem. Phys.* **2005**, *122*, 214507−214515.
(33) Nugent, S.; Ladanyi, B. M. *J. Chem. Phys.* **2004**, *120*, 874−884.
(34) Stubbs, J. M.; Siepmann, J. I. *J. Chem. Phys.* **2004**, *121*, 1525−1534.
(35) Saharay, M.; Balasubramanian, S. *J. Chem. Phys.* **2004**, *120*, 9694−9702.
(36) Raveendran, P.; Ikushima, Y.; Wallen, S. L. *Acc. Chem. Res.* **2005**, *38*, 478−485.
(37) Zhang, Y.; Yang, J.; Yu, Y. *J. Phys. Chem. B* **2005**, *109*, 13375−13382.
(38) Car, R.; Parrinello, M. *Phys. Rev. Lett.* **1985**, *55*, 2471−2474.
(39) Hutter, J.; Ballone, P.; Bernasconi, M.; Focher, P.; Fois, E.; Goedecker, S.; Marx, D.; Parrinello, M.; Tuckerman, M. E. CPMD Version 3.9.1, Max Planck Institut fuer Festkoerperforschung, Stuttgart, and IBM Zurich Research Laboratory, 1990−2005.
(40) Tuckerman, M. E.; Yarne, D. A.; Samuelson, S. O.; Hughes, A. L.; Martyna, G. *J. Comput. Phys. Commun.* **2000**, *128*, 333−376.
(41) Becke, A. D. *Phys. Rev. A* **1988**, *38*, 3098−3100.
(42) Lee, C.; Yang, W.; Parr, R. G. *Phys. Rev. B* **1988**, *37*, 785−789.
(43) Morrone, J. A.; Tuckerman, M. E. *J. Chem. Phys.* **2002**, *117*, 4403−4413.
(44) Troullier, N.; Martins, J. L. *Phys. Rev. B* **1991**, *43*, 1993−2006.
(45) Frisch, M. J.; Trucks, G. W.; Schlegel, H. B.; Scuseria, G. E.; Robb, M. A.; Cheeseman, J. R.; Zakrzewski, V. G.; Montgomery, J. A., Jr.; Stratmann, R. E.; Burant, J. C.; Dapprich, S.; Millam, J. M.; Daniels, A. D.; Kudin, K. N.; Strain, M. C.; Farkas, O.; Tomasi, J.; Barone, V.; Cossi, M.; Cammi, R.; Mennucci, B.; Pomelli, C.; Adamo, C.; Clifford, S.; Ochterski, J.; Petersson, G. A.; Ayala, P. Y.; Cui, Q.; Morokuma, K.; Malick, D. K.; Rabuck, A. D.; Raghavachari, K.; Foresman, J. B.; Cioslowski, J.; Ortiz, J. V.; Stefanov, B. B.; Liu, G.; Liashenko, A.; Piskorz, P.; Komaromi, I.; Gomperts, R.; Martin, R. L.; Fox, D. J.; Keith, T.; Al-Laham, M. A.; Peng, C. Y.; Nanayakkara, A.; Gonzalez, C.; Challacombe, M.; Gill, P. M. W.; Johnson, B. G.; Chen, W.; Wong, M. W.; Andres, J. L.; Head-Gordon, M.; Replogle, E. S.; Pople, J. A. *Gaussian 98*, revision A.9; Gaussian, Inc.: Pittsburgh, PA, 1998.
(46) Becke, A. D. *J. Chem. Phys.* **1993**, *98*, 5648−5652.
(47) MacKerell, A. D.; Bashford, D.; Bellott, M.; Dunbrack, R. L.; Evanseck, J. D.; Field, M. J.; Fischer, S.; Gao, J.; Guo, H.; Ha, S.; Joseph-McCarthy, D.; Kuchnir, L.; Kuczera, K.; Lau, F. T. K.; Mattos, C.; Michnick, S.; Ngo, T.; Nguyen, D. T.; Prodhom, B.; Reiher, W. E.; Roux, B.; Schlenkrich, M.; Smith, J. C.; Stote, R.; Straub, J.; Watanabe, M.; Wiorkiewicz-Kuczera, J.; Yin, D.; Karplus, M. *J. Phys. Chem. B* **1998**, *102*, 3586−3616.
(48) Harris, J. G.; Yung, K. H. *J. Phys. Chem.* **1995**, *99*, 12021−12024.
(49) Martyna, G. J.; Klein, M. L.; Tuckerman, M. *J. Chem. Phys.* **1992**, *97*, 2635−2643.
(50) Chen, B.; Potoff, J. J.; Siepmann, J. I. *J. Phys. Chem. B* **2001**, *105*, 3093−3104.
(51) Stubbs, J. M.; Siepmann, J. I. *J. Am. Chem. Soc.* **2005**, *127*, 4722−4729.
(52) Chen, J.; Shaka, A. J.; Mandelshtam, V. A. *J. Magn. Reson.* **2000**, *147*, 129−137.
(53) Knozinger, E.; Beichert, P. *J. Phys. Chem.* **1995**, *99*, 4906−4911.
(54) Laasonen, K.; Sprik, M.; Parrinello, M. *J. Chem. Phys.* **1993**, *99*, 9080−9089.
(55) Chandra, A. *Phys. Rev. Lett.* **2000**, *85*, 768−771.
(56) Allen. M. P.; Tildesley, D. J. *Computer Simulation of Liquids*; Clarendon Press: Oxford, 1987.
(57) Cabaco, M. I.; Danten, Y.; Tassaing, T.; Longelin, S.; Besnard, M. *Chem. Phys. Lett.* **2005**, *413*, 258−262.
(58) Kazarian, S. G.; Vincent, M. F.; Bright, F. V.; Liotta, C. L.; Eckert, C. A. *J. Am. Chem. Soc.* **1996**, *118*, 1729−1736.
(59) Figure 3B of Yee et al.[20] exhibits multiple peaks for the vibrational spectrum in the $\nu_2$ bending region of pure $scCO_2$ at 40 °C and 400 bar. The splittings were, however, not commented upon in this original work.
(60) Meredith, J. C.; Johnston, K. P.; Seminario, J. M.; Kazarian, S. G.; Eckert, C. A. *J. Phys. Chem.* **1996**, *100*, 10837−10848.
(61) Perdew, J. P.; Burke, K.; Ernzerhof, M. *Phys. Rev. Lett.* **1996**, *77*, 3865−3868.